

# Linearized electrooptic microwave downconversion using phase modulation and optical filtering

Vincent R. Pagán,<sup>1,2,\*</sup> Bryan M. Haas,<sup>1</sup> and T. E. Murphy<sup>2,3</sup>

<sup>1</sup>Laboratory for Physical Sciences, College Park, MD 20740, USA

<sup>2</sup>Dept. of Electrical & Computer Engineering,  
University of Maryland, College Park, MD 20740, USA

<sup>3</sup>Institute for Research in Electronics & Applied Physics,  
University of Maryland, College Park, MD 20740, USA

[\\*vrpagan@lps.umd.edu](mailto:vrpagan@lps.umd.edu)

**Abstract:** We propose and demonstrate an electrooptic technique for relaying microwave signals over an optical fiber and downconverting the microwave signal to an intermediate frequency at the receiver. The system uses electrooptic phase modulation in the transmitter to impose the microwave signal on an optical carrier followed by re-modulation with a microwave local oscillator at the receiver. We demonstrate that by subsequently suppressing the optical carrier using a notch filter, the resulting optical signal can be directly detected to obtain a downconverted microwave signal. We further show that by simply controlling the amplitude of the microwave local oscillator, the system can be linearized to third-order, yielding an improvement in the dynamic range.

© 2011 Optical Society of America

**OCIS codes:** (060.5625) Radio frequency photonics; (060.5060) Phase modulation; (230.0250) Optoelectronics; (060.0060) Fiber optics and optical communications.

---

## References and links

1. J. Capmany and D. Novak, "Microwave photonics combines two worlds," *Nat. Photonics* **1**, 319–330 (2007).
2. A. J. Seeds and K. J. Williams, "Microwave Photonics," *J. Lightwave Technol.* **24**, 4628–4641 (2006).
3. L. M. Johnson and H. V. Roussel, "Reduction of intermodulation distortion in interferometric optical modulators," *Opt. Lett.* **13**, 928–930 (1988).
4. S. K. Korotky and R. M. de Ridder, "Dual Parallel Modulation Schemes for Low-Distortion Analog Optical Transmission," *IEEE J. Sel. Areas Comm.* **8**, 1377–1381 (1990).
5. M. L. Farwell, Z.-Q. Lin, E. Wooten, and W. S. C. Chang, "An Electrooptic Intensity Modulator with Improved Linearity," *IEEE Photon. Technol. Lett.* **3**, 792–795 (1991).
6. M. Nazarathy, J. Berger, A. J. Ley, I. M. Levi, and Y. Kagan, "Progress in Externally Modulated AM CATV Transmission Systems," *J. Lightwave Technol.* **11**, 82–105 (1993).
7. W. B. Bridges and J. H. Schaffner, "Distortion in Linearized Electrooptic Modulators," *IEEE Trans. Microw. Theory Tech.* **43**, 2184–2197 (1995).
8. G. E. Betts and F. J. O'Donnell, "Microwave Analog Optical Links Using Suboctave Linearized Modulators," *IEEE Photon. Technol. Lett.* **8**, 1273–1275 (1996).
9. Y. Chiu, B. Jalali, S. Garner, and W. Steier, "Broad-Band Electronic Linearizer for Externally Modulated Analog Fiber-Optic Links," *IEEE Photon. Technol. Lett.* **11**, 48–50 (1999).
10. E. I. Ackerman, "Broad-Band Linearization of a Mach-Zehnder Electrooptic Modulator," *IEEE Trans. Microw. Theory Tech.* **47**, 2271–2279 (1999).
11. B. M. Haas and T. E. Murphy, "A Simple, Linearized, Phase-Modulated Analog Optical Transmission System," *IEEE Photon. Technol. Lett.* **19**, 729–731 (2007).

12. B. Masella, B. Hraimel, and X. Zhang, "Enhanced Spurious-Free Dynamic Range Using Mixed Polarization in Optical Single Sideband Mach-Zehnder Modulator," *J. Lightwave Technol.* **27**, 3034–3041 (2009).
13. T. S. Tan, R. L. Jungerman, and S. S. Elliott, "Optical Receiver and Modulator Frequency Response Measurement with a Nd:YAG Ring Laser Heterodyne Technique," *IEEE Trans. Microw. Theory Tech.* **37**, 1217–1222 (1989).
14. A. K. M. Lam, M. Fairburn, and N. A. F. Jaeger, "Wide-Band Electrooptic Intensity Modulator Frequency Response Measurement Using an Optical Heterodyne Down-Conversion Technique," *IEEE Trans. Microw. Theory Tech.* **54**, 240–246 (2006).
15. G. K. Gopalakrishnan, W. K. Burns, and C. H. Bulmer, "Microwave-Optical Mixing in LiNbO<sub>3</sub> Modulators," *IEEE Trans. Microw. Theory Tech.* **41**, 2383–2391 (1993).
16. A. C. Lindsay, G. A. Knight, and S. T. Winnall, "Photonic Mixers for Wide Bandwidth RF Receiver Applications," *IEEE Trans. Microw. Theory Tech.* **43**, 2311–2317 (1995).
17. C. K. Sun, R. J. Orazi, S. A. Pappert, and W. K. Burns, "A Photonic-Link Millimeter Wave Mixer Using Cascaded Optical Modulators and Harmonic Carrier Generation," *IEEE Photon. Technol. Lett.* **8**, 1166–1168 (1996).
18. R. Helkey, J. C. Twichell, and C. Cox III, "A Down-Conversion Optical Link with RF Gain," *J. Lightwave Technol.* **15**, 956–961 (1997).
19. K.-I. Kitayama and R. A. Griffin, "Optical Downconversion from Millimeter-Wave to IF-Band Over 50-km-Long Optical Fiber Link Using an Electroabsorption Modulator," *IEEE Photon. Technol. Lett.* **11**, 287–289 (1999).
20. F. Zeng and J. Yao, "All-Optical Microwave Mixing and Bandpass Filtering in a Radio-Over-Fiber Link," *IEEE Photon. Technol. Lett.* **17**, 899–901 (2005).
21. Y. Le Guennec, G. Maury, J. Yao, and B. Cabon, "New Optical Microwave Up-Conversion Solution in Radio-Over-Fiber Networks for 60-GHz Wireless Applications," *J. Lightwave Technol.* **24**, 1277–1282 (2006).
22. Y. Li, D. Yoo, P. Herczfeld, A. Rosen, A. Madjar, and S. Goldwasser, "Receiver for coherent fiber-optic link with high dynamic range and low noise figure," in "Proceedings of Topical Meeting on Microwave Photonics," (2005).
23. V. J. Urlick, F. Bucholtz, P. S. Devgan, J. D. McKinney, and K. J. Williams, "Phase Modulation With Interferometric Detection as an Alternative to Intensity Modulation With Direct Detection for Analog-Photonic Links," *IEEE Trans. Microw. Theory Tech.* **55**, 1978–1985 (2007).
24. A. Ramaswamy, L. A. Johansson, J. Klamkin, H.-F. Chou, C. Sheldon, M. J. Rodwell, L. A. Coldren, and J. E. Bowers, "Integrated Coherent Receivers for High-Linearity Microwave Photonic Links," *J. Lightwave Technol.* **26**, 209–216 (2008).
25. T. R. Clark and M. L. Dennis, "Coherent Optical Phase-Modulation Link," *IEEE Photon. Technol. Lett.* **19**, 1206–1208 (2007).
26. G. Qi, J. Yao, J. Seregelyi, S. Paquet, and C. Belisle, "Optical Generation and Distribution of Continuously Tunable Millimeter-Wave Signals Using an Optical Phase Modulator," *J. Lightwave Technol.* **23**, 2687–2695 (2005).
27. H. Chi, X. Zou, and J. Yao, "Analytical Models for Phase-Modulation-Based Microwave Photonic Systems With Phase Modulation to Intensity Modulation Conversion Using a Dispersive Device," *J. Lightwave Technol.* **27**, 511–521 (2009).
28. B. Chen, S. L. Zheng, X. M. Zhang, X. F. Jin, and H. Chi, "Simultaneously realizing PM-IM conversion and efficiency improvement of fiber-optic links using FBG," *J. Electromagn. Waves Appl.* **23**, 161–170 (2009).
29. R. D. Esman and K. J. Williams, "Wideband Efficiency Improvement of Fiber Optic Systems by Carrier Subtraction," *IEEE Photon. Technol. Lett.* **7**, 218–220 (1995).
30. M. Attygalle, C. Lim, G. J. Pendock, A. Nirmalathas, and G. Edvell, "Transmission Improvement in Fiber Wireless Links Using Fiber Bragg Gratings," *IEEE Photon. Technol. Lett.* **17**, 190–192 (2005).
31. A. R. Chraplyvy, R. W. Tkach, L. L. Buhl, and R. C. Alferness, "Phase Modulation to Amplitude Modulation Conversion of CW Laser Light in Optical Fibres," *Electron. Lett.* **22**, 409–411 (1986).
32. A. F. Elrefaie, R. E. Wagner, D. A. Atlas, and D. G. Daut, "Chromatic Dispersion Limitations in Coherent Lightwave Transmission Systems," *J. Lightwave Technol.* **6**, 704–709 (1988).
33. U. Gliese, S. Nørskov, and T. N. Nielsen, "Chromatic Dispersion in Fiber-Optic Microwave and Millimeter-Wave Links," *IEEE Trans. Microw. Theory Tech.* **44**, 1716–1724 (1996).
34. G. H. Smith, D. Novak, and Z. Ahmed, "Overcoming Chromatic-Dispersion Effects in Fiber-Wireless Systems Incorporating External Modulators," *IEEE Trans. Microw. Theory Tech.* **45**, 1410–1415 (1997).

---

## 1. Introduction

Radio-over-fiber (RoF) systems allow radio frequency (RF) signals to be relayed over optical fiber and are particularly attractive for applications where microwave signals must be transmitted over distances in which coaxial cable would be prohibitively lossy [1, 2]. One of the key challenges of designing RoF links is finding ways to modulate and demodulate the microwave signal onto an optical carrier without introducing distortion or nonlinearities. Several methods

have been demonstrated to produce linearized electrooptic (EO) modulation such as using two or more modulators, multiple wavelengths, different polarization states, signal predistortion, or feed-forward circuitry [3–12]. For many applications, it is also desirable to downconvert the microwave signal to a lower intermediate frequency (IF) at the receiver so that it can be more easily digitized. In conventional systems, downconversion is achieved using an electrical mixer, which can further contribute to the loss and distortion of the link. An alternative is to perform downconversion optically by employing heterodyne detection [13, 14] or EO mixing [15–21].

Here we demonstrate a new RoF architecture that addresses the aforementioned challenges by using a combination of EO phase modulation and optical filtering. Unlike intensity modulators, phase modulators do not require active bias control circuitry which can result in a simpler link design. Phase modulation has recently attracted attention for RoF applications, with several groups reporting systems for demodulation based on coherent detection or feedback loops [11, 22–25]. The main disadvantage of phase modulation has been the complexity of detecting the phase encoded information at the receiver. However, it has been shown that phase modulated signals can be converted to intensity modulation by inserting a dispersive device or by filtering the optical carrier after phase modulation [26–28]. The intensity modulated signal can then be detected using a square-law photoreceiver. Furthermore, suppression of the optical carrier in intensity modulated links has been shown to have the added benefit of increasing the effective modulation depth, which results in improvements in the RF-to-RF gain [28–30].

Here we show that by using two cascaded phase modulators, one driven by a microwave input signal and the other by a strong microwave local oscillator (LO) tone, a downconverted signal can be produced at the difference frequency. Because the downconversion is accomplished through EO mixing and optical filtering, the photoreceiver need only be fast enough to resolve the downconverted IF signal. Slower photoreceivers are not only more economical, but may also be able to handle higher optical powers, which could further lead to additional improvements of the link gain and noise figure. The system presented in this paper achieves a downconversion gain that is up to 2.64 dB higher than that of a non-downconverting intensity modulated link with comparable components and optical power.

A surprising feature of the system is that by simply adjusting the amplitude of the microwave LO, it is possible to eliminate the third-order intermodulation distortion (IMD3) introduced by the modulation and demodulation processes. This linearization method does not require multiple wavelengths, additional modulators, polarization states, or precise splitting of the optical and RF powers, and can be implemented entirely in the receiver. Despite a penalty in the downconversion gain, we show that the linearized system increases the spur-free dynamic range (SFDR) from 103.5 dB/Hz<sup>2/3</sup> to 114.0 dB/Hz<sup>4/5</sup>.

## 2. Principle of operation

Figure 1 shows a diagram of the downconverting phase-modulated RoF link presented here. A high stability, narrow linewidth, fiber laser (NP Photonics) with a center wavelength of 1552.470 nm was used as the optical source. The output of the laser was connected to the transmitter (TX) phase modulator through polarization maintaining fiber (PMF). The TX phase modulator was a 40 GHz, z-cut LiNbO<sub>3</sub> modulator with a measured  $V_{\pi}$  of 5.3 V at 20 GHz. The output of the TX phase modulator was connected to the input of the receiver (RX) phase modulator through a second length of PMF. The RX phase modulator was similar to the TX phase modulator, but it had a measured  $V_{\pi}$  of 4.1 V at 19.5 GHz. The transmitter and receiver phase modulators were driven by a microwave input signal and a strong microwave LO tone, respectively.

The signal emerging from the RX phase modulator was sent through a fiber Bragg grating (FBG) in transmission mode to suppress the optical carrier. The FBG was designed for add/drop

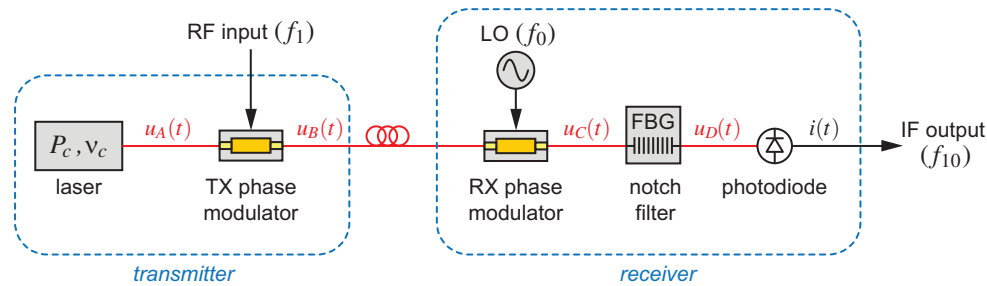


Fig. 1. Diagram of the downconverting RoF link presented here. The system uses two cascaded optical phase modulators, one in the transmitter and one in the receiver, followed by a fiber Bragg grating (FBG) and a square-law photoreceiver. The FBG is chosen to suppress the optical carrier at  $\nu_c$ . The receiver phase modulator is driven by a strong microwave LO to produce IF beat products that are detected by an optical photoreceiver.

filtering of dense wavelength division multiplexing systems having 25 GHz channel spacings. This filter provided approximately 23 dB attenuation to the carrier with respect to the sidebands at 1552.470 nm and approximately 2.5 dB of out-of-band insertion loss. The 3 dB notch-width of the FBG was measured to be approximately 14 GHz and the frequency offset between the optical carrier and the filter center frequency was less than 1 GHz. The optical output from the filter was connected to an InGaAs PIN photodiode having a  $50 \Omega$  internal termination resistor and a nominal 3 dB bandwidth of 12 GHz.

Figure 2 illustrates the downconversion process by showing the optical and electrical spectra measured at various points in the link. The optical spectra were captured using a high resolution Brillouin optical spectrum analyzer (Aragon Photonics) with a spectral resolution of 80 fm (10 MHz). The fiber laser spectrum is shown in Fig. 2(a) where  $P_c$  denotes the optical carrier power. At the transmitter, the optical signal is modulated by a weak 20 GHz microwave signal with modulation depth  $m_1 \approx 0.1$ . This produces a series of optical sidebands with intensities proportional to  $J_l^2(m_1)$  at frequencies of  $lf_1$  about the optical carrier where  $l = 0, \pm 1, \pm 2, \dots$  as shown in Fig. 2(b).

In the receiver, the phase modulated optical signal is re-modulated by a strong microwave LO having a modulation depth  $m_0 \approx 1.08$  and frequency  $f_0 = 19.6$  GHz. This generates additional optical sidebands with frequency spacings of  $mf_0$ , where  $m = 0, \pm 1, \pm 2, \dots$ , about each of the  $lf_1$  frequency components. The resulting spectrum is shown in Fig. 2(c) where each spectral component is proportional to  $J_l^2(m_1)J_m^2(m_0)$ .

The twice-modulated optical signal is then sent through a FBG with the measured optical transmission shown in Fig. 2(d). The FBG filters out the optical carrier for which  $l + m = 0$  while allowing the sidebands to pass. The carrier-suppressed optical spectrum is shown in Fig. 2(e).

After the notch filter, the resulting optical signal is detected by a square-law photoreceiver. As explained later in Section 3, the photocurrent contains terms at the downconverted frequency,  $\Omega_{10} = \Omega_1 - \Omega_0$ , that are proportional to the power of the microwave input signal. Fig. 2(f) shows the measured electrical spectrum of the photodetected signal which is clearly centered at the downconverted frequency of  $f_{10} = 400$  MHz.

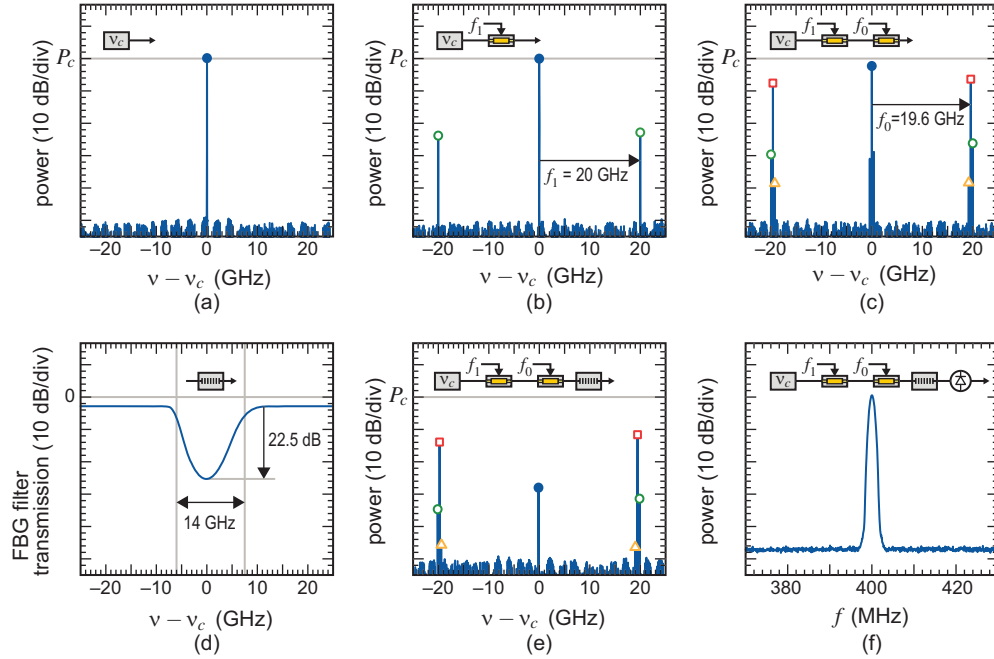


Fig. 2. (a) Optical spectrum of the laser (closed circle). (b) Optical spectrum measured after the transmitter phase modulator, showing the optical carrier (closed circle) and sidebands at  $\pm f_1 = \pm 20$  GHz (open circles). (c) Optical spectrum measured after the receiver phase modulator driven by a LO, showing additional sidebands at  $\pm f_0 = \pm 19.6$  GHz (open squares),  $\pm f_1 \mp 2f_0 = \pm 19.2$  GHz (open triangles), and  $\pm f_1 \mp f_0 = \pm 400$  MHz (no symbol). (d) Measured transmission of the FBG. (e) Optical spectrum measured after the FBG, showing suppression of the optical carrier and sidebands at  $\pm f_1 \mp f_0 = \pm 400$  MHz. (f) Electrical spectrum measured at the photodetector, showing the downconverted tone at  $f_{10} = 400$  MHz.

### 3. Theoretical analysis

We begin with a continuous wave optical signal with optical frequency  $\omega_c$ , that can be described by the complex optical field

$$u_A(t) = \sqrt{P_c} e^{j\omega_c t} \quad (1)$$

where we have normalized the field such that  $|u_A|^2$  represents the optical power. For simplicity, in the analysis that follows, we neglect the optical insertion losses of the modulators, filter, and transmission fiber. These losses can be accounted for by proportionately reducing  $P_c$ . Alternatively, one may define  $P_c$  to be the optical power measured at the input of the receiver modulator when the signal and LO are turned off.

In the transmitter, the signal is phase modulated by a sinusoidal microwave signal with amplitude  $V_1$  and frequency  $\Omega_1$  to produce an optical field

$$u_B(t) = \sqrt{P_c} e^{j\omega_c t} e^{jm_1 \sin \Omega_1 t} \quad (2)$$

where  $m_1$  is the input signal modulation depth, expressed in radians as

$$m_1 = \pi \frac{V_1}{V_\pi} \quad (3)$$

and  $V_\pi$  is the half-wave voltage of the phase modulator. At the receiver, the signal is remodulated by a strong microwave LO tone to give

$$u_C(t) = \sqrt{P_c} e^{j\omega_c t} e^{jm_1 \sin \Omega_1 t} e^{jm_0 \sin \Omega_0 t} \quad (4)$$

where  $m_0$  is the modulation depth produced by the LO, defined analogously to Eq. (3). Applying the Jacobi-Anger expansion to Eq. (4), we obtain

$$u_C(t) = \sqrt{P_c} e^{j\omega_c t} \sum_l \sum_m J_l(m_1) J_m(m_0) e^{j(l\Omega_1 + m\Omega_0)t} \quad (5)$$

where both summations run from  $-\infty$  to  $+\infty$ .

The optical notch filter can be mathematically modeled by excluding those terms in Eq. (5) for which  $l + m = 0$ ,

$$u_D(t) = \sqrt{P_c} e^{j\omega_c t} \sum_l \sum_{\substack{m \\ (l+m \neq 0)}} J_l(m_1) J_m(m_0) e^{j(l\Omega_1 + m\Omega_0)t} \quad (6)$$

Following the FBG notch filter, the optical field is detected by a square-law photoreceiver with responsivity  $R$  to produce a photocurrent given by

$$i(t) = R|u_D(t)|^2 = RP_c \sum_l \sum_m \sum_n \sum_p \left[ J_l(m_1) J_m(m_0) J_n(m_1) J_p(m_0) e^{j[(l-n)\Omega_1 + (m-p)\Omega_0]t} \right] \quad (7)$$

$(l+m \neq 0)(n+p \neq 0)$

To determine the downconversion gain of the system, we consider only the terms in Eq. (7) that are oscillating at the downconverted frequency  $\Omega_{10} \equiv \Omega_1 - \Omega_0$ . This is equivalent to including only the terms in the summation for which  $(l - n) = \pm 1$  and  $(m - p) \mp 1$ , i.e.,

$$i(t)|_{\omega=\Omega_{10}} = RP_c \sum_l \sum_{m \neq -l} J_l(m_1) J_{l+1}(m_1) J_m(m_0) J_{m-1}(m_0) e^{j\Omega_{10}t} + \text{c.c.} \quad (8)$$

The restricted summation in Eq. (8) can be written as a difference of two full summations,

$$i(t)|_{\omega=\Omega_{10}} = RP_c \left[ \sum_l \sum_m J_l(m_1) J_{l+1}(m_1) J_m(m_0) J_{m-1}(m_0) \right] \quad (9a)$$

$$- \sum_m J_{-m}(m_1) J_{-m+1}(m_1) J_m(m_0) J_{m-1}(m_0) \left] e^{j\Omega_{10}t} + \text{c.c.} \quad (9b)$$

The double-summation in Eq. (9a) can be interpreted as the photocurrent that would result if the notch filter was absent. Applying a Bessel summation identity, this contribution can be shown to be zero, which confirms that phase modulation by itself cannot be directly detected by a square-law photoreceiver. Thus, the downconverted photocurrent simplifies to

$$i(t)|_{\omega=\Omega_{10}} = I_{10} \cos \Omega_{10}t \quad (10)$$

where the photocurrent amplitude,  $I_{10}$ , is defined as

$$I_{10} \equiv 2RP_c \sum_m J_m(m_1) J_{m-1}(m_1) J_m(m_0) J_{m-1}(m_0) \quad (11)$$

Taylor expanding Eq. (11) to third-order in  $m_1$  yields

$$I_{10} = RP_c \left[ 2m_1 J_0(m_0) J_1(m_0) - \frac{m_1^3}{4} (3J_0(m_0) J_1(m_0) - J_1(m_0) J_2(m_0)) \right] \quad (12)$$

For small microwave signals applied to the TX phase modulator (i.e.  $m_1 \ll 1$ ), the cubic term in Eq. (12) can be ignored. The time-averaged downconverted electrical output power at  $\Omega_{10}$  through an impedance  $Z_{\text{out}}$  is then

$$P_{\text{out}} = 2Z_{\text{out}} [RP_c m_1 J_0(m_0) J_1(m_0)]^2 \quad (13)$$

Using Eq. (3), the time-averaged input microwave power at  $\Omega_1$  through an impedance  $Z_{\text{in}}$  can be written as

$$P_{\text{in}} = \frac{1}{2Z_{\text{in}}} \left( \frac{m_1 V_\pi}{\pi} \right)^2 \quad (14)$$

The small-signal RF-to-IF downconversion gain of the system is found by taking the ratio of Eq. (13) to Eq. (14) to obtain

$$G = \left( \frac{2\pi RP_c}{V_\pi} \right)^2 [J_0(m_0) J_1(m_0)]^2 Z_{\text{out}} Z_{\text{in}} \quad (15)$$

The gain in Eq. (14) can be compared to that of a non-downconverting quadrature-biased Mach-Zehnder (MZ) link having the same input optical power, impedances and half-wave voltage, which can be shown to be

$$G_{\text{MZ}} = \left( \frac{\pi RP_c}{2V_\pi} \right)^2 Z_{\text{out}} Z_{\text{in}} \quad (16)$$

It should be noted that a quadrature-biased Mach-Zehnder link is not equivalent to the phase-modulated link presented here because (a) it uses only one EO intensity modulator, instead of two EO phase modulators, and could therefore provide a lower overall optical insertion loss (b) it would require an electrical mixer to downconvert the transmitted signal to IF, which would introduce additional electrical losses not present in our link. Nonetheless, the comparison is useful because it allows one to factor out common component related parameters such as photodiode responsivity, transmitter modulator half-wave voltage, and input and output electrical impedances, which affect the link architectures in the same way. The small-signal gain given in Eq. (15) can then be expressed in terms of  $G_{\text{MZ}}$  as

$$G = 16 [J_0(m_0) J_1(m_0)]^2 G_{\text{MZ}} \quad (17)$$

The gain in Eq. (17) is maximized for a LO modulation depth of  $m_0 \cong 1.08$ . In this case, the link presented here achieves a downconversion gain that is a factor of  $1.84 \times$  (2.64 dB) higher than that of a comparable MZ modulator link.

#### 4. Linearization

As explained in Section 3, the downconversion gain of the RoF link presented here can be maximized by setting the amplitude of the LO to  $m_0 = 1.08$ . However, the gain is only one factor that governs the overall link performance. In some situations, it may be preferable to optimize the linearity and dynamic range by minimizing the intermodulation distortion (IMD). For sub-octave signals, the dynamic range is limited by third-order intermodulation distortion (IMD3). This distortion can easily be characterized by applying two closely-spaced microwave tones at the RF input. The fundamental tones and the IMD products can then be measured in the downconverted electrical spectrum.

Intermodulation distortion is associated with nonlinearities in the EO modulation and demodulation transfer functions. Even in the single tone case, distortion is present in the downconverted photocurrent at  $\Omega_{10}$  as evident in the term proportional to  $m_1^3$  in Eq. (12). This contribution to signal distortion can be eliminated by appropriately choosing the LO modulation

depth  $m_0$ , which leads to the following linearization condition:

$$3J_0(m_0)J_1(m_0) - J_1(m_0)J_2(m_0) = 0 \quad (18)$$

As shown in Appendix A, in the two-tone analysis, this condition also eliminates the IMD3 products at  $2f_1 - f_2 - f_0$  and  $2f_2 - f_1 - f_0$ . The smallest value of  $m_0$  that solves Eq. (18) was numerically found to be  $m_0 = 2.17$ . When this value of  $m_0$  is substituted into Eq. (17), the downconversion gain evaluates to  $G = 0.081 G_{MZ}$ , which is 13.6 dB lower than for the maximum gain case.

To experimentally confirm this result, we conducted a two-tone measurement in which the LO strength ( $m_0$ ) was swept while the power of the downconverted fundamental tones and third order intermodulation (IMD3) were measured. For these measurements, the single microwave tone at the TX phase modulator shown in Fig. 1 was replaced by a pair of closely spaced tones with frequencies  $f_1 = 20.00$  GHz and  $f_2 = 20.02$  GHz and equal modulation depths  $m_1 = m_2 = 0.14$ . In order to improve the electrical isolation between the two synthesizers, three-port ferrite circulators configured as electrical isolators were used at the synthesizer outputs. The two microwave tones were then combined using a four-port hybrid coupler. The LO frequency was set to  $f_0 = 19.6$  GHz to produce downconverted tones at 400 and 420 MHz and sub-octave IMDs at 380 and 440 MHz. The DC photocurrent, downconverted fundamental power, and downconverted IMD power were measured as a function of the LO modulation depth.

Figure 3 shows the results of this measurement along with the corresponding theoretically calculated curves. When calculating the output powers for Fig. 3, an additional factor of 1/4 was incorporated to account for the presence of an internal 50  $\Omega$  terminating resistor in the photoreceiver. The measurements and theory show excellent agreement across all values of  $m_0$ . It is clear that the fundamental power is maximized at  $m_0 = 1.08$  while the IMD3 power is minimized by choosing  $m_0 = 2.17$ , which reduces the fundamental power by 13.6 dB relative to its maximum value.

Figure 4(a) shows the electrical spectrum measured for a LO modulation depth of  $m_0 = 1.08$ , which produces the maximum downconversion gain. The IMD products are clearly visible at frequencies of  $2f_1 - f_2 - f_0 = 380$  MHz and  $2f_2 - f_1 - f_0 = 440$  MHz. To linearize the system, we increased the LO power to achieve  $m_0 = 2.17$ , which produced the electrical spectrum shown in Fig. 4(b). The fundamental tones are reduced by 13.8 dB from their value in Fig. 4(a), which agrees well with the theoretically calculated gain penalty of 13.6 dB, and the IMD products fell below the noise floor of the electrical spectrum analyzer. Finally, we increased the input signal powers by +13.8 dB to compensate for the linearization gain penalty. As shown in Fig. 4(c), even in this case, the IMD products are suppressed relative to the non-linearized case shown in Fig. 4(a). This confirms that, despite the gain penalty, this linearization technique can improve the dynamic range.

When the IMD3 products are suppressed by choosing  $m_0$  according to Eq. (18), the residual sub-octave IMD products are expected to be dominated by fifth-order contributions. Thus, we do not expect complete suppression of the IMD products in the linearized case, but only the elimination of the third-order dependence. To verify this, we measured the downconverted and IMD powers as a function of the input power. Figure 5 shows the results of these measurements for the maximum gain and linearized cases. The solid curves were simulated while the circles indicate experimentally measured points. The dashed curves and open circles correspond to the maximum-gain case,  $m_0 = 1.08$ , and the green curves and filled circles indicate the linearized case,  $m_0 = 2.17$ . For the latter case, the IMD products clearly have a fifth-order dependence on the input power, indicating that the third-order dependence has in fact been suppressed. All measurements in Fig. 5 were performed using a resolution bandwidth of 100 kHz. The IMD products were measured using a low-noise IF preamplifier and tunable RF bandpass filter at

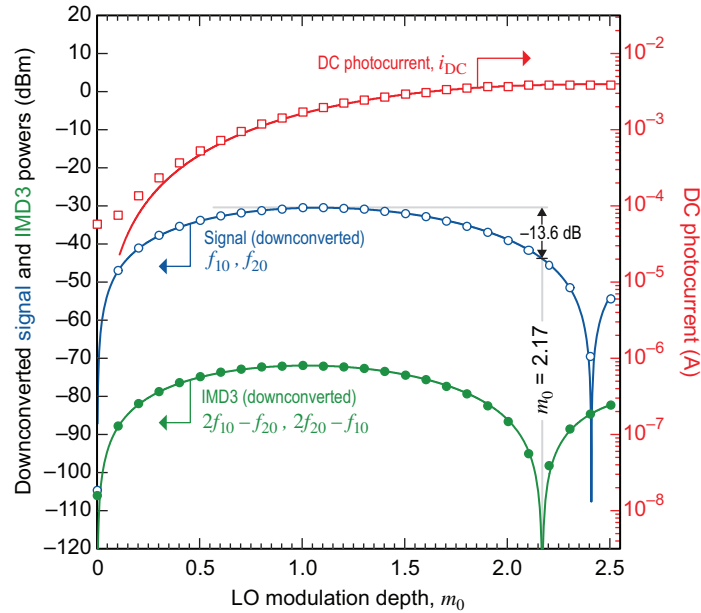


Fig. 3. Calculated (solid lines) and measured DC photocurrent (squares), downconverted signal power (open circles), and third-order intermodulation distortion (IMD3) power (filled circles) as a function of the LO modulation depth  $m_0$ . The downconverted signal and IMD3 powers grow in proportion to  $m_1$  and  $m_1^3$ , respectively, but here they are evaluated at an input modulation depth of  $m_1 = 0.14$ .

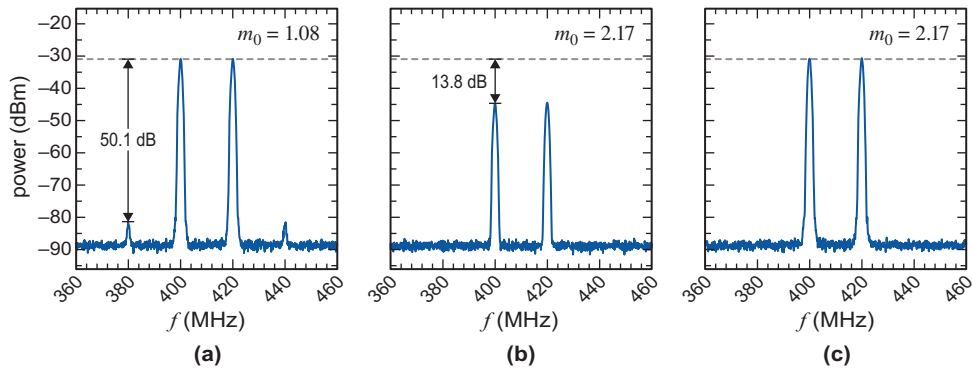


Fig. 4. Measured downconverted electrical spectra, showing the suppression of intermodulation distortion products achieved by adjusting the LO strength  $m_0$ . (a) Downconverted spectrum obtained when the LO power was adjusted for maximum gain (i.e.,  $m_0 = 1.08$ ). (b) Spectrum obtained under same conditions as (a), but with the LO amplitude increased to  $m_0 = 2.17$ . (c) Output spectrum obtained under same conditions as in (b), but with the input signal strength increased by +13.8 dB to compensate for the gain penalty. Notice that even when the input amplitude is increased to compensate for the gain penalty, the dynamic range is improved in comparison to the non-linearized case shown in (a).

the output of the photodetector to isolate the weaker IMD tones from the stronger fundamental tones and to overcome the poor noise figure of the spectrum analyzer. Despite the gain penalty, the linearized system achieves a normalized dynamic range of  $114.0 \text{ dB/Hz}^{4/5}$ , whereas the maximum-gain case reaches only  $103.5 \text{ dB/Hz}^{2/3}$ .

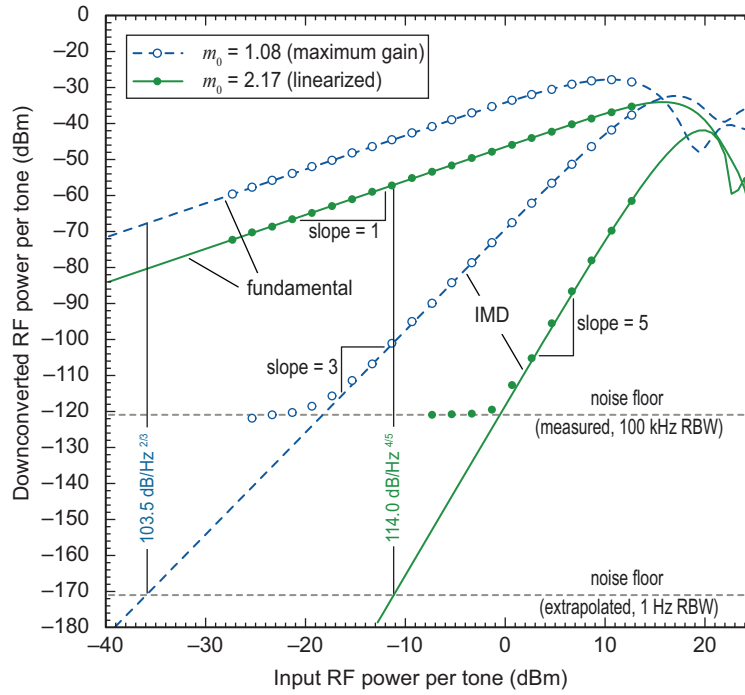


Fig. 5. Downconverted signal and intermodulation powers as a function of the input microwave power. The blue curves and open symbols were obtained with a LO amplitude of  $m_0 = 1.08$ , which gives the highest downconversion gain. The green curves and filled symbols were obtained with  $m_0 = 2.17$ , which suppresses the third-order intermodulation distortion.

## 5. System bandwidth

When calculating the gain of the downconverting link in Section 3, we assumed an ideal notch filter that completely extinguished all terms in the vicinity of the carrier while fully transmitting all of the spectral sidebands. Furthermore, we neglected the effects of chromatic dispersion that occurs as the optical signal propagates in the fiber linking the transmitter and receiver. In this section, we address these topics, both of which can place a bound on the bandwidth of the system.

Theoretically, the bandwidth of the optical notch filter limits the minimum frequency that can be transmitted through the system. To experimentally investigate this effect, we measured the downconversion gain as a function of the input signal frequency,  $f_1$ . The LO frequency was adjusted in parallel with the input signal frequency in order to maintain a constant downconverted IF of  $f_1 - f_0 = 400 \text{ MHz}$ . Since the half-wave voltage of EO modulators vary with frequency, the LO power was adjusted to maintain a constant LO modulation depth of  $m_0 = 1.08$  for all measurements. When varying the signal frequency  $f_1$ , the half-wave voltage  $V_\pi$  was independently measured so that the electrical response of the TX phase modulator could also be factored out.

Figure 6 shows the normalized downconversion gain as a function of the signal frequency  $f_1$ . The gain was normalized relative to the reference value given by Eq. (16), which represents the gain of a Mach-Zehnder (MZ) intensity-modulated link with comparable parameters. As before, the normalization was adjusted by 6 dB to properly account for the presence of an internal 50  $\Omega$  terminating resistor in the photoreceiver. This normalization process implicitly factors out the electrical response of the modulator, by incorporating the measured frequency dependence in  $V_\pi$ . The dashed line in Fig. 6 shows the 2.64 dB downconversion gain (relative to the MZ case) obtained from theory, under the assumption of ideal filtering. When the input modulation frequency exceeds the half the notch filter bandwidth, the experimentally measured gain closely approaches this theoretical value. As shown in Fig. 2(d), the FBG had a spectral bandwidth of approximately 14 GHz. Therefore, when the input modulation frequency falls below 7 GHz, the  $\pm 1$  sidebands are partially blocked by the filter, causing the downconversion gain to decrease, as shown in Fig. 6.

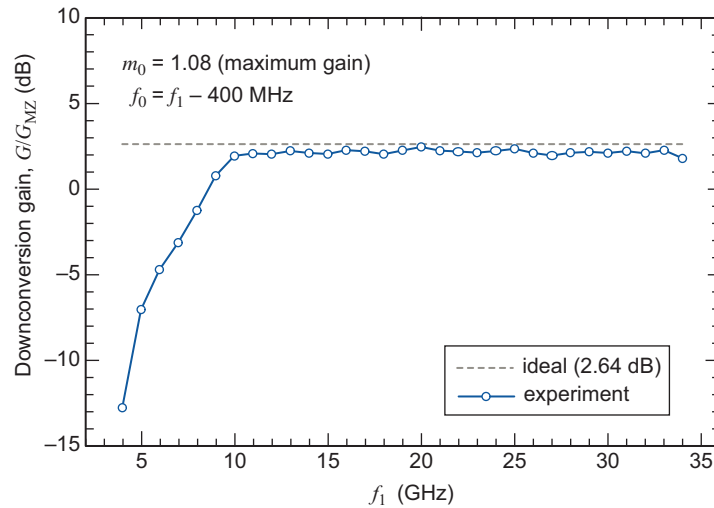


Fig. 6. Downconversion gain as a function of the signal carrier frequency  $f_1$ , normalized relative to  $G_{MZ}$ , the gain of a comparable non-downconverting link employing a quadrature-biased Mach-Zehnder intensity modulator with direct detection.

Chromatic dispersion in the fiber is well-known to produce phase modulation to intensity modulation conversion, and vice versa [31–34]. In systems where the modulation frequencies are known, an appropriately chosen dispersive medium inserted after a phase modulator can be used in place of the optical notch filter to achieve EO frequency mixing [20, 21, 27].

This system, however, is designed to accommodate a wide range of possible input frequencies. In this case, chromatic dispersion limits the bandwidth, transmission length, and downconversion gain. The derivation presented in Section 3 can be generalized to include the effect of chromatic dispersion between the transmitter and receiver. If the two phase modulators are separated by a fiber of length  $L$ , then to first-order, the amplitude of the downconverted photocurrent can be shown to be

$$I_{10} = 2RP_c m_1 J_0(m_0) J_1(m_0) \cos\left(\frac{\pi LD}{c} \lambda_c^2 f_1^2\right) \quad (19)$$

where  $D$  is the chromatic dispersion of the fiber, typically expressed in ps/nm·km,  $\lambda_c$  is the carrier wavelength, and  $f_1$  is the signal frequency. Apart from the additional sinusoidal factor, Eq. (19) is seen to be identical to the leading linear term in Eq. (12).

The downconverted signal will be completely extinguished when the dispersion and frequency satisfy the following relation:

$$\frac{2L|D|}{c} \lambda_c^2 f_1^2 = 1, 3, 5, \dots \quad (20)$$

For the case of  $D = 17$  ps/nm km,  $\lambda_c = 1552.470$  nm, and  $f_1 = 20$  GHz, the first null occurs at a fiber length of  $L = 9.15$  km, and the  $-3$  dB point occurs at  $L = 4.58$  km.

Conversely, for a given fiber length, chromatic dispersion limits the maximum frequency that can be transmitted. The downconversion gain is reduced by  $-3$  dB at a frequency of

$$f_1 = \frac{1}{2\lambda_c} \sqrt{\frac{c}{L|D|}} \quad (21)$$

Another configuration of interest is when the input signal and LO modulators are both co-located at the transmitter, which is then separated from the FBG and photodetector by a dispersive fiber. In this case, the analysis of the downconversion gain is slightly more complex [27]. Numerical simulations suggest, however, that although fading can occur under these conditions, the signal fading criterion is dictated primarily by the downconverted IF,  $f_1 - f_0$ . Using  $f_1 = 20$  GHz,  $f_0 = 19.6$  GHz and  $m_0 = 1.08$ , we numerically calculate that the first null in transmission should occur at a length of  $L \simeq 200$  km.

## 6. Conclusions

In this paper, we reported a downconverting radio-over-fiber system that employs two cascaded optical phase modulators followed by an optical notch filter for carrier suppression. The system offers several advantages over competing downconversion schemes. Unlike conventional electrical downconversion, the system does not require a high-speed photoreceiver or electrical mixer. In contrast to optical heterodyne downconversion methods, the system does not require two phase-locked optical sources. Because it does not use intensity modulators, active bias control is not needed. We further demonstrated that by simply adjusting the strength of the microwave LO, it is possible to eliminate the third-order intermodulation distortion in the system, which is shown to improve the dynamic range of the link.

### A. Two-Tone Analysis

In Section 3, expressions for the downconversion gain for the single tone case were derived up to third-order. In this Appendix, the case where the input signal is comprised of two closely spaced tones is considered. The fundamental, IMDs, and DC terms are evaluated up to fifth-order.

At the transmitter, an optical carrier with power  $P_c$  and frequency  $\omega_c$  is phase modulated by two closely spaced sinusoidal tones  $v_1(t) = V_1 \sin \Omega_1 t$  and  $v_2(t) = V_2 \sin \Omega_2 t$ , to produce an optical field given by

$$u_B(t) = \sqrt{P_c} e^{j\omega_c t} e^{jm_1 \sin \Omega_1 t} e^{jm_2 \sin \Omega_2 t} \quad (22)$$

where, as before, the  $i^{\text{th}}$  modulation depth (in radians) is given by  $m_i \equiv \pi V_i / V_\pi$ . At the receiver, the signal is modulated again by a strong LO tone with modulation depth  $m_0$  and frequency  $\Omega_0$ , to produce an optical field given by

$$u_C(t) = \sqrt{P_c} e^{j\omega_c t} e^{jm_1 \sin \Omega_1 t} e^{jm_2 \sin \Omega_2 t} e^{jm_0 \sin \Omega_0 t} \quad (23)$$

The exponentials in Eq. (23) are expanded in terms of Bessel functions to obtain

$$u_C(t) = \sqrt{P_c} e^{j\omega_c t} \sum_l \sum_m \sum_n J_l(m_1) J_m(m_2) J_n(m_0) e^{j(l\Omega_1 + m\Omega_2 + n\Omega_0)t} \quad (24)$$

An ideal optical notch filter will extinguish all of the terms in Eq. (24) for which  $l + m + n = 0$ , i.e.,

$$u_D(t) = \sqrt{P_c} e^{j\omega_c t} \sum_l \sum_m \sum_n J_l(m_1) J_m(m_2) J_n(m_0) e^{j(l\Omega_1 + m\Omega_2 + n\Omega_0)t} \quad (25)$$

( $l+m+n \neq 0$ )

The detected photocurrent is then given by

$$i(t) = R |u_D(t)|^2 \quad (26)$$

$$= RP_c \sum_l \sum_m \sum_n \sum_p \sum_q \sum_r J_l(m_1) J_m(m_2) J_n(m_0) J_p(m_1) J_q(m_2) J_r(m_0) \quad (27)$$

( $l+m+n \neq 0$ )( $p+q+r \neq 0$ )

$$\times e^{j[(l-p)\Omega_1 + (m-q)\Omega_2 + (n-r)\Omega_0]t}$$

Expanding Eq. (27) up to fifth-order in  $m_1$  and  $m_2$ , and retaining only the downconverted in-band products and DC terms, we find

$$i(t) = RP_c \left\{ \left[ \Phi_0(m_0) + \Phi_2(m_0)(m_1^2 + m_2^2) + \Phi_4(m_0)(m_1^4 + 4m_1^2 m_2^2 + m_2^4) \right] \right. \quad (28)$$

$$\left. + \left[ \Phi_1(m_0)m_1 + \Phi_3(m_0)(m_1^3 + 2m_1 m_2^2) + \Phi_5(m_0)(m_1^5 + 6m_1^3 m_2^2 + 3m_1 m_2^4) \right] \cos(\Omega_{10}t) \right. \quad (29)$$

$$\left. + \left[ \Phi_3(m_0)m_1^2 m_2 + \Phi_5(3m_1^2 m_2^3 + 2m_1^4 m_2) \right] \cos((2\Omega_{10} - \Omega_{20})t) \right. \quad (30)$$

$$\left. + \Phi_5(m_0)m_1^3 m_2^2 \cos((3\Omega_{10} - 2\Omega_{20})t) \right. \quad (31)$$

$$\left. + \text{similar terms at } \Omega_{20}, (2\Omega_{20} - \Omega_{10}) \text{ and } (3\Omega_{20} - 2\Omega_{10}) \right\}$$

where  $\Omega_{ij} \equiv (\Omega_i - \Omega_j)$  and the coefficients  $\Phi_n(m_0)$  are tabulated below:

$\Phi_0(m_0)$	$1 - J_0^2(m_0)$	(32)
$\Phi_1(m_0)$	$2J_0(m_0)J_1(m_0)$	
$\Phi_2(m_0)$	$\frac{1}{2} [J_0^2(m_0) - J_1^2(m_0)]$	
$\Phi_3(m_0)$	$-\frac{1}{4} [3J_0(m_0)J_1(m_0) - J_1(m_0)J_2(m_0)]$	
$\Phi_4(m_0)$	$-\frac{1}{32} [3J_0^2(m_0) - 4J_1^2(m_0) + J_2^2(m_0)]$	
$\Phi_5(m_0)$	$\frac{1}{96} [10J_0(m_0)J_1(m_0) - 5J_1(m_0)J_2(m_0) + J_0(m_0)J_1(m_0)]$	

We note that the linearization condition given by Eq. (18) is equivalent to requiring  $\Phi_3(m_0) = 0$ , which eliminates not only the third-order IMD products in Eq. (30), but also the cubic contribution to the fundamental tones in Eq. (29).

Equation (31) indicates that there will be fifth-order intermodulation products present at the downconverted frequency  $3\Omega_{10} - 2\Omega_{20}$ . For clarity, these terms were not plotted in Fig. 5, because for  $m_1 = m_2$  they are always smaller than the dominant IMD3 contributions at  $2\Omega_{10} - \Omega_{20}$  for small input signals ( $m_1, m_2 \ll 1$ ).